NDT&E International ▮ (▮▮▮▮) ▮▮▮–▮▮▮

Contents lists available at ScienceDirect

NDT&E International

journal homepage: www.elsevier.com/locate/ndteint

Modeling and testing of high frequency GPR data for evaluation of structural deformation

Luciana Orlando [a,*], Alessia Pezone [a], Alessandro Colucci [b]

[a] Department Idraulica Trasporti e Strade, 'Sapienza' Rome University, Italy
[b] Department Dynamic and Environmental Tests, ENEA-FIM-MATQUAL, Casaccia, Rome, Italy

ARTICLE INFO

Article history:
Received 27 July 2009
Received in revised form
23 November 2009
Accepted 24 November 2009

Keywords:
2 GHz antenna
Reflection
Transillumination
Deformation detection
Hollow pier

ABSTRACT

The paper describes the application, on a hollow pier, of a high frequency multi-component 2 GHz GPR antenna for the evaluation of deformation induced by mechanical stress. The study, performed in the laboratory, was made on a reinforced concrete hollow pier built to scale 1:5. The GPR survey data were obtained before and after the mechanical stress application, in reflection and transillumination modes. The data interpretation was supported by a GPR theoretical model of a pier. The interpretation of the GPR reflection data was very challenging as the iron rods used to reinforce the pier led to wave diffraction and the air inter-space inside the pier itself produced multiple reflections. No continuous fractures were revealed, probably because the stress caused only micro-fractures. This assumption was supported by analyses of the time slices from reflection data and the first direct wave arrival times from transillumination data. In the second survey we observed increased reflectivity in the time slices and decreased first arrival times of the direct wave, with respect to the first survey. The theoretical GPR data carried out on the physical model, which reproduced the actual pier, were found to be very useful tools for interpreting the actual data as they allow signal to noise separation.

1. Introduction

The objective of this study was to test the capability of a high frequency multi-component georadar (2 GHz) to detect the inner structures of a hollow pier, and to evaluate deformation produced by induced seismic events.

The test was performed in a laboratory on a typical hollow pier normally used in the construction of viaducts and bridges in Europe. Even today there are no accurate seismic codes for piers like these, and the effect of seismic stress on such structures is still not very well known. Indeed, the lack of a project code becomes evident when one considers the collapse of such structures under seismic strain, the collapse often being due to shearing stress, iteration cut-bending and inadequate lap-splice. Therefore it is clearly important to develop new structural-restoration methods for repairing and reinforcing hollow piers, given the considerable diffusion of such piers in transportation infrastructures throughout Europe. Thus, it is of primary importance to develop new, non-invasive methods for the inspection, detection, mapping, and monitoring of conditions during pier assessment, and for an evaluation of the effectiveness of any structural restoration carried out.

The objective of the paper was to analyse the most common damage caused by seismic events on a typical square hollow pier built according to traditional design criteria, criteria that do not always conform with current seismic codes. Bending stress under normally controlled conditions was taken into account. The laboratory tests simulating seismic stress were performed on a purposely built hollow pier, scale 1:5, which was subjected to traction applied to its head. Seismic tests contribute, in a very valid way, to the formulation of a global model for evaluating seismic response of hollow bridge-piers.

The non-invasive techniques normally used for the inspection, detection, mapping and monitoring of conditions in the assessment of rock, remains and structures are sonic tests [1,2], seismic refraction [3], seismic tomography [4] and GPR [1,5–13]. Recently, GPR was used for the monitoring over time of the assessment conditions of a historical building and pavement, by Orlando [14] and Giannopoulos [15].

Because of the complex geometry of the pier in this study, we considered the most suitable method for the inspection and detection of cracks to be high frequency GPR.

GPR surveys of the pier were conducted before and after the application of mechanical stress, and the data were acquired and processed using the same parameters and codes, thus

* Corresponding author.
E-mail address: luciana.orlando@uniroma1.it (L. Orlando).

0963-8695/$ - see front matter © 2009 Elsevier Ltd. All rights reserved.
doi:10.1016/j.ndteint.2009.11.006

highlighting any possible deformation of the pier. The GPR data acquired before and after the mechanical test were compared, in order to show the capability and the limitations of the georadar method for evaluating effects induced by seismic events on bridge-piers.

2. Pier geometry and seismic test

The hollow pier, built to a scale 1:5, was constructed with reinforced concrete and is 1.5 m high with a square section of 0.36 m (Fig. 1a). The inner hollow air section is square in shape (Fig. 1b), the sides measuring 0.24 m from 0 to 1.1 m height, and 0.06 m from 1.1 to 1.5 m.

The reinforcing rods are 8 and 10 mm in diameter (Fig. 1c), and there are 16 vertical and 21 horizontal bars forming a regularly spaced grid. The pier is anchored to a plinth with U-bolt longitudinal reinforcements (Fig. 1d).

Excluding the plinth, the pier geometry is

- 1.50 m high
- Base size: 0.36×0.36 m.
- Air inter-space from bottom to 1.1 m: 0.24×0.24 m
- Thickness of concrete from bottom to 1.1 m: 0.06 m.
- Air inter-space from 1.1 m to top: 0.06×0.06 m
- Longitudinal reinforcement: 16 iron U-bolts with diameter of 10 mm.
- Transversal reinforcement: 21 iron rods with diameter of 8 mm.

For the mechanical test the pier was reinforced with high resistance carbon fiber, from the bottom to a height of 0.60 m (Fig. 1d).

For the reinforcement carbon fiber was preferred, rather than the more common glass fiber used for confinement intervention, so as to reduce damage due to air pollution and atmospheric agents.

The seismic test consisted of traction applied to the pier head by a hydraulic actuator. The actuator, which operates at 0.05 mm/s in displacement rate control, was bound to the top of the pier (Fig. 2). Using the actuator, we applied a vertical force of 80 kN to the pier to simulate real seismic strain. The test started from the neutral position and stopped when the force applied by the actuator reached a value of less than −20% of the maximum force. Fig. 2 shows the lay-out scheme.

Strain effect was measured with:

- 6 vertical laser transducers
- 1 wire mechanic transducer on the pier head (LF1)

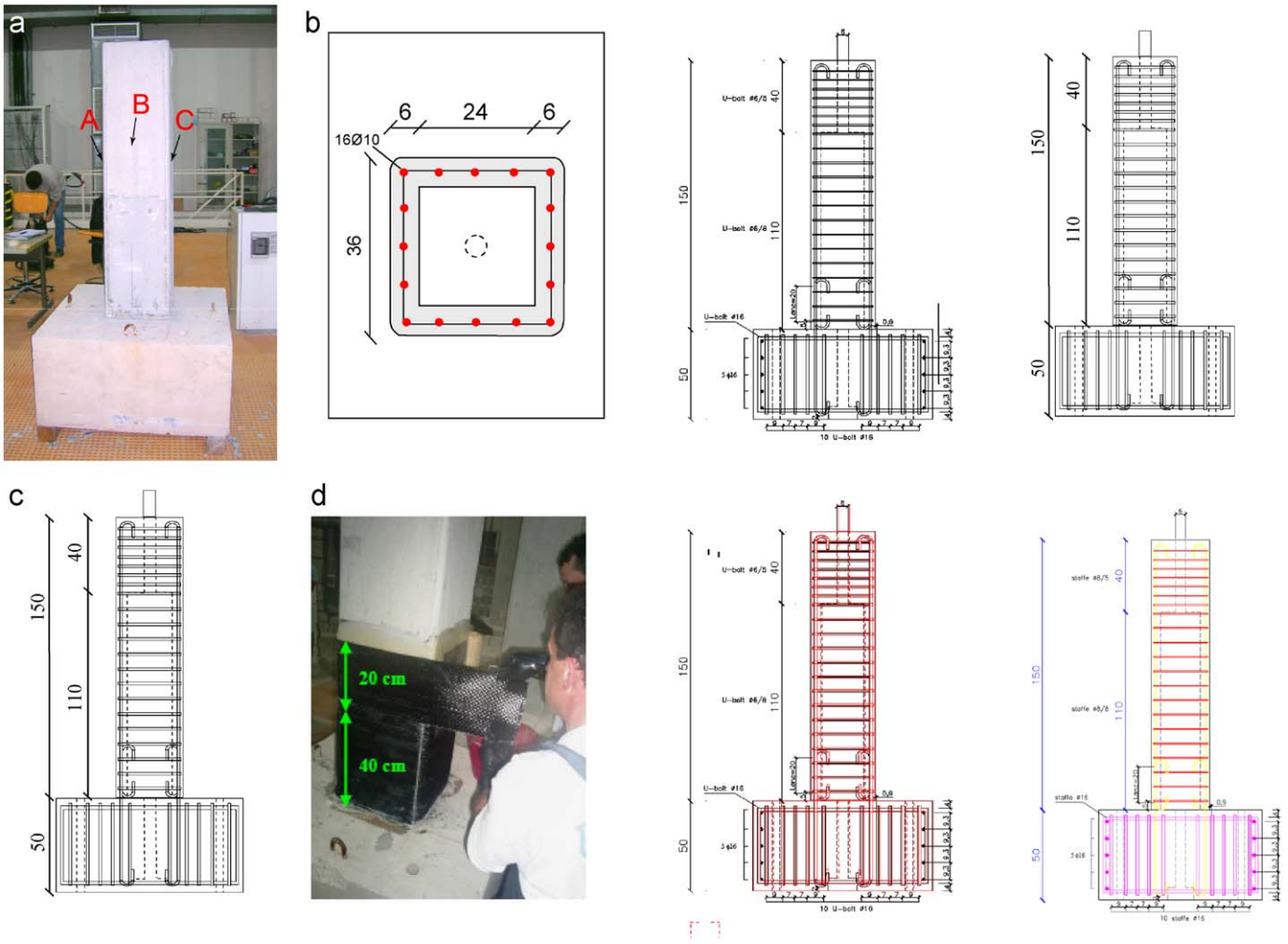

Fig. 1. (a) Photograph of the hollow pier used in the study; (b) square bottom of the pier; (c) scheme of reinforced iron rods; (d) carbon fiber reinforcement from 0 to 0.60 m.

Please cite this article as: Orlando L, et al. Modeling and testing of high frequency GPR data for evaluation of structural deformation. NDT&E Int (2010), doi:10.1016/j.ndteint.2009.11.006

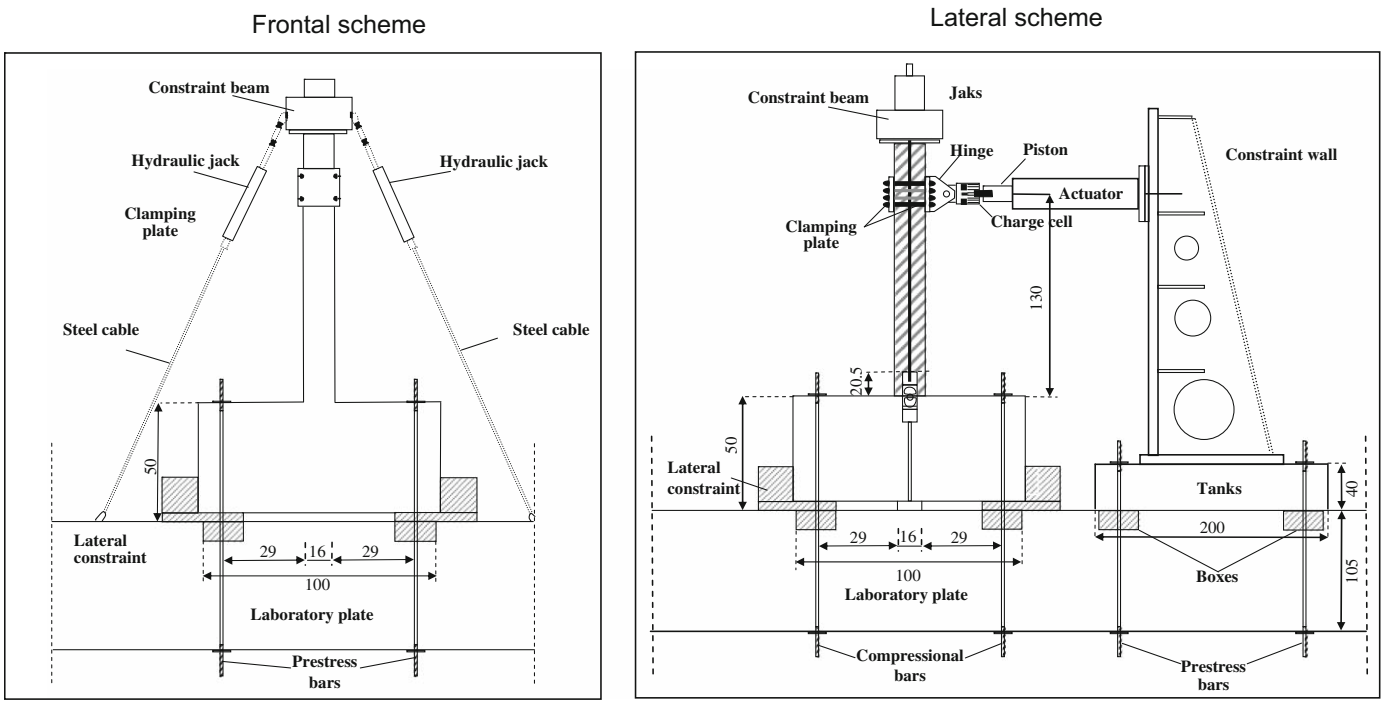

Fig. 2. Left—frontal test lay-out; right—lateral test lay-out.

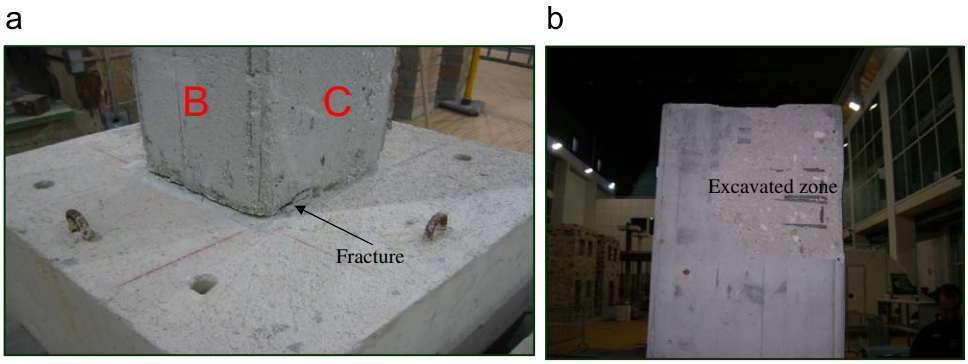

Fig. 3. (a) Fracture induced by strain at the pier–plinth contact. (b) Concrete excavation induced by actuator on the pier head.

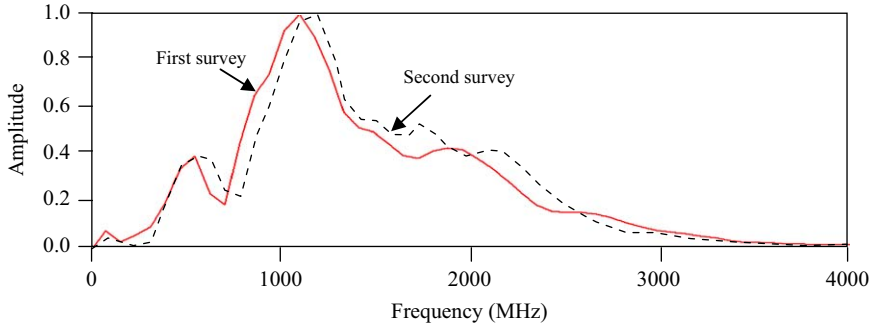

Fig. 4. Normalized amplitude frequency spectra of data of first survey (continuous line) and second survey (dashed line).

- 8 extensometers
- 1 load cell on the actuator

The stress applied to the pier did not induce any visible damage to the structure except for the fracture at the contact between pier and plinth (Fig. 3a), and for the concrete excavation, induced by the actuator, on one side of the head pier (Fig. 3b).

3. Theoretical modeling

Because of the complex geometries of the pier and the reduced dimensions of the concrete layers forming the pier structure, which are at the limit of resolution for the 2 GHz antenna, theoretical reflection georadar modelling was carried out. A discussion follows on the theoretical georadar data simulating

Please cite this article as: Orlando L, et al. Modeling and testing of high frequency GPR data for evaluation of structural deformation. NDT&E Int (2010), doi:10.1016/j.ndteint.2009.11.006

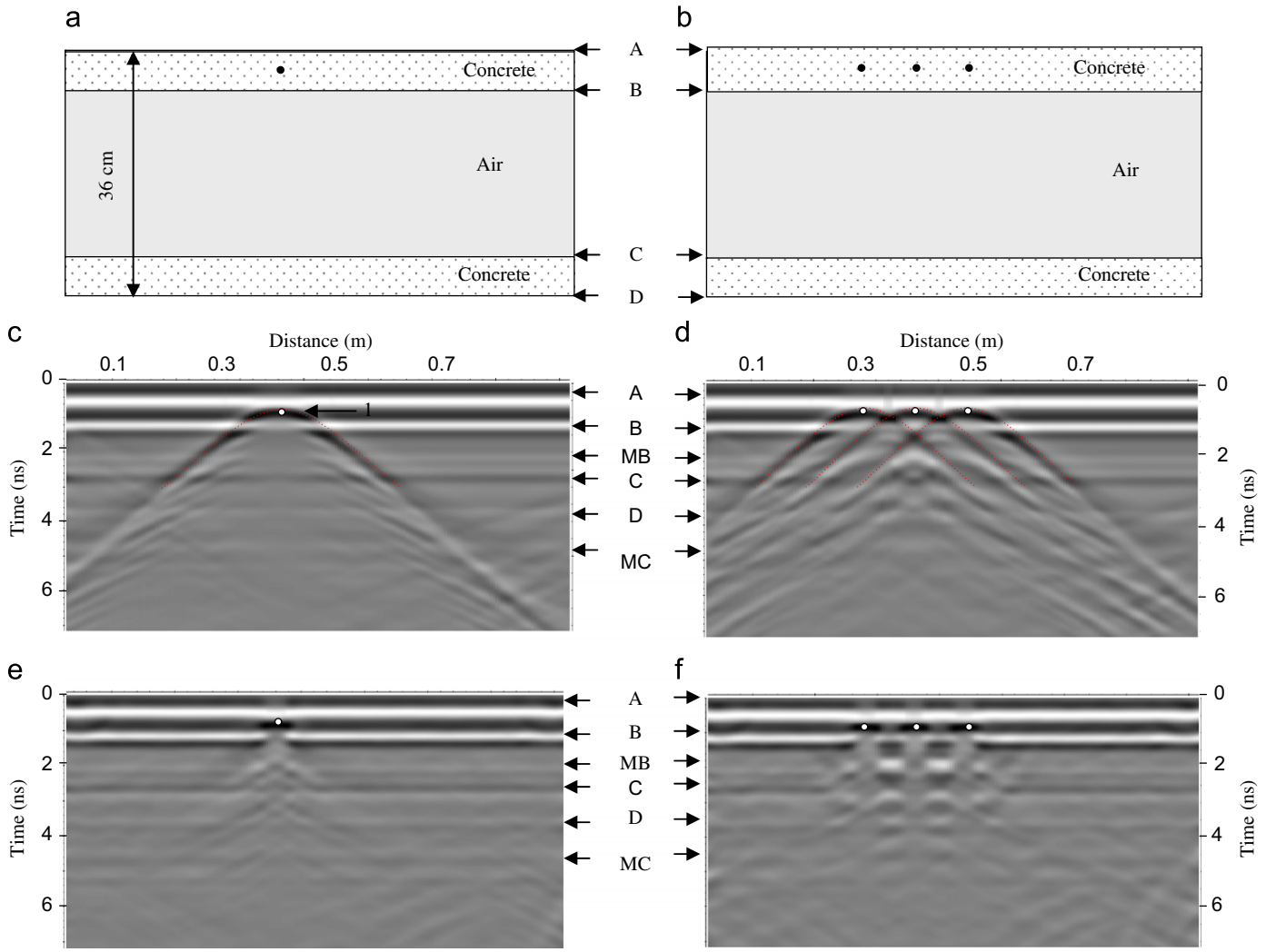

Fig. 5. Pier model 0.36 m thick, reinforced with iron rods: one rod (a), three rods (b) used for GPR simulations (c and d). In (e) and (f) the data migrated with the Stolt algorithm. (A and B) Top and bottom of first concrete layer. (C and D) Top and bottom of second concrete layer; MB=multiple of B; MC=multiple of C.

a full and a hollow pier reinforced with iron bars and a pier with an oblique fracture.

The theoretical data were the result of calculations based on a finite difference approximation algorithm in the time domain FDTD, GprMax2D v.2.0 [16]. Note that the code solves the Maxwell equations for electric and magnetic vector fields as a function of time and space, and the equations are solved as a function of the model geometry, the constitutive parameters of the medium, the starting conditions, antenna parameters and sampling rate (time and space).

The problem is approached in a 2-dimensional space with the assumptions summarized below:

- All media are homogeneous and isotropic.
- The transmitter antenna is a linear source.
- The constitutive parameters of media are unrelated to the frequency.

The modelling was performed using a Ricker wavelet, peak frequency 1100 MHz, and by assigning to the concrete a relative permittivity (ε_r) of 6, conductivity (σ) of 0.01 S/m and relative permeability (μ_r) of 1. The Ricker peak frequency of 1100 MHz was taken into account on the basis of a spectral analysis of the actual data (Fig. 4) acquired on the studied pier before and after the stress application. The spectra show a peak frequency of 1100 and 1200 MHz for the first and second surveys respectively, and frequencies of up to 2800 MHz for both surveys. The signal wave length for an actual peak frequency of 1.2 GHz, and an e.m. velocity of 0.12 m/ns is 0.10 m, a wave length shorter than that for the concrete layer of the pier.

Theoretical data were calculated for several models, starting from the simplest and going to the most complex. The most significant models are discussed here.

The GPR simulation of the pier, with a square section of 0.36 m formed by concrete reinforced with one or three iron rods with an inner hollow of 0.24 m, is shown in Fig. 5a, b. The iron rods, diameter 0.01 m, lie at a depth of 0.03 m from the surface and are spaced 0.08 m apart (Fig. 5a, b). On the basis of the modelling, and taking into account the e.m. velocity of 12.24 cm/ns used in the modelling, the two travel times of reflection and multiples are calculated and marked with arrows and letters on the GPR theoretical images (Fig. 5). Even though the models generating the images are known, the GPR data (Fig. 5c, d) are difficult to interpret. The direct wave (A), reflection from the first interface (B), and the diffraction from the rod partly overlap. The rods produce primary and multiple diffractions which interfere with each other and with the reflections from the interfaces, both constructively and destructively. The rods are easily detectable from the primary diffraction hyperbola (mapped with dashed

Please cite this article as: Orlando L, et al. Modeling and testing of high frequency GPR data for evaluation of structural deformation. NDT&E Int (2010), doi:10.1016/j.ndteint.2009.11.006

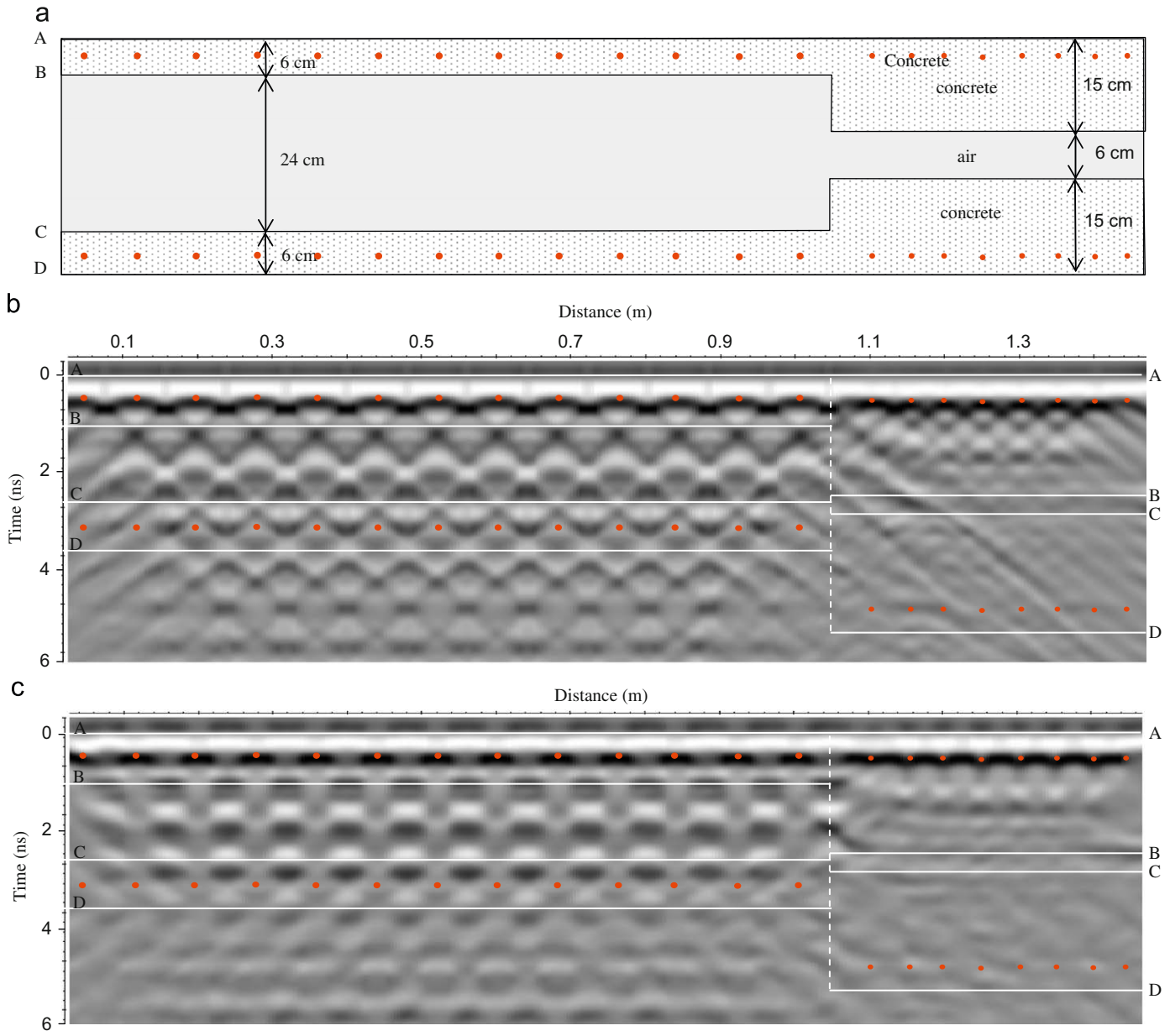

Fig. 6. (a) Pier model with geometry the same as actual pier. (b) GPR section of model. (c) Migrated section of data in (b). (A and B) Top and bottom of first concrete layer. (C and D) Top and bottom of the second concrete layer.

lines in Fig. 5). The model with 3 rods shows that the interference of the diffraction hyperbola produces organized anomalies that can be interpreted as actual objects. To improve the resolution of the section, the migration algorithm based on the Stolt code [17], using a constant velocity of 12.5 cm/ns, was applied to the data. The migrated sections (Fig. 5e and f) are no clearer than the unmigrated ones because also the diffracted energies of multiple diffraction hyperbola are focused, giving rise to several anomalies which are not related to any actual object. The reflection from the concrete–air interface (B) appears as a dashed line.

The complexity of the GPR images for these models depends on (i) the overlapping of the direct air wave with the diffraction hyperbola induced by the rods and the proximity of the rods to the antenna position, (ii) the interference of the diffraction hyperbolas between themselves and with the opposite interfaces, (iii) ghost anomalies produced by the constructive interference of diffraction hyperbola and (iv) discontinuity of planar reflectors behind the rods, produced by the shielding effect of rods. From the theoretical modeling, it can be ascertained that the actual GPR data are very difficult to interpret without *a priori* knowledge of the inner structure of the pier.

Fig. 6 shows the theoretical GPR profile (b) of the hollow pier, which has geometry similar (a) to that used in the actual georadar survey that took into account only the transversal rods, normal to the profile direction. The complexity of the GPR image is increased with respect to the model of Fig. 5. To facilitate the interpretation, the time model of the geometries generating the theoretical model of the pier, obtained with irradiation from the top, is mapped on the GPR image (lines in the figure). It can be observed that (i) it is not easy to discriminate between anomalies due to true interfaces and the organized noise produced by the destructive and constructive interference of the diffracted energy of the iron rods and the layer interfaces, (ii) the rods are very near to the signal resolution, and (iii) direct and reflected waves interfere with each other and with reflected signals from the rods. Another important element inhibiting the interpretation

Please cite this article as: Orlando L, et al. Modeling and testing of high frequency GPR data for evaluation of structural deformation. NDT&E Int (2010), doi:10.1016/j.ndteint.2009.11.006

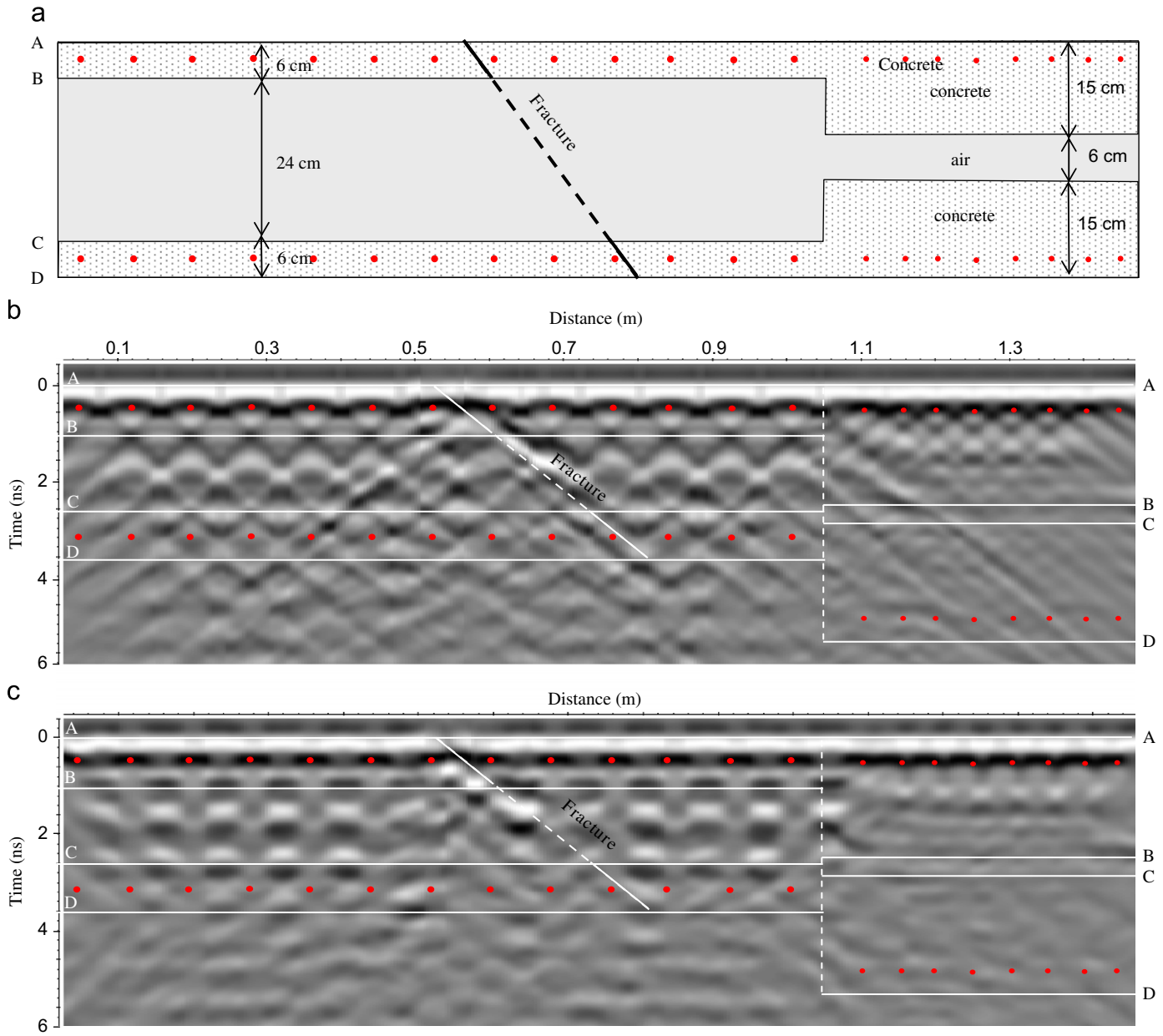

Fig. 7. (a) Pier model with geometry the same as actual pier, simulating a fracture. (b) GPR section of model. (c) Migrated section of data in (b). (A and B) Top and bottom of the first concrete layer. (C and D) Top and bottom of the second concrete layer.

is the perfect symmetry of the rods and the layers forming the pier. The migrated section (Fig. 6c) fails to reduce the ambiguity in the interpretation of the section because the interference among the diffraction hyperbola themselves, and with the concrete–air interfaces (lines B, C and D in Fig. 6), produces anomalies quite similar to true ones that also fall within the air inter-space.

Let us now discuss a theoretical model of a pier with an oblique plane fracture. Fig. 7b shows the GPR section generated by the model of Fig. 7a. The crack has a slope of 45° and a displacement of 2 millimetres.

The GPR image shows that the crack is detectable only by diffraction hyperbola induced by the edge of the crack and the disarrangement of the organized anomalies of the rods and concrete–air interfaces. The migrated data (Fig. 7c) focus the diffraction energy, but do not improve the section's image quality very much, because of the same problem described for the previous model.

The GPR image of the actual hollow pier reveals that, despite the knowledge achieved through the pier model, the data interpretation is still a very challenging task as it is difficult to separate actual anomalies from what are induced by the constructive and destructive interference of the signals and multiples.

4. Georadar surveys

The GPR surveys were performed with an IDS Corporation instrument equipped with a 2 GHz bipolar antenna (Fig. 8a), with the two dipoles placed normal to each other (Fig. 8b). The instrument allows the acquisition of a four-component electric field at the same point, with parallel broadside y-directed antennas (channel 1), parallel broadside *x*-directed antennas (channel 2), a perpendicular antenna *y*-directed source and an *x*-directed receiver (channel 3), and a perpendicular antenna *x*-directed source and

Please cite this article as: Orlando L, et al. Modeling and testing of high frequency GPR data for evaluation of structural deformation. NDT&E Int (2010), doi:10.1016/j.ndteint.2009.11.006

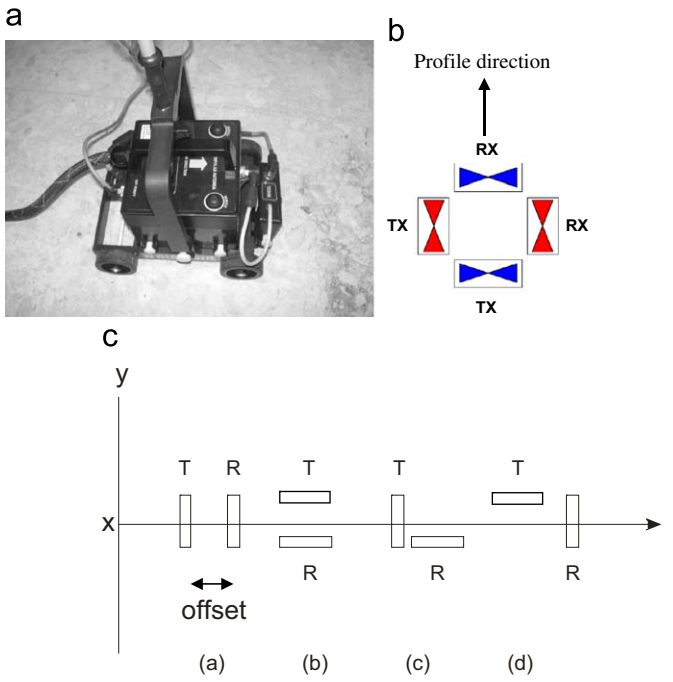

Fig. 8. (a) 2 GHz bipolar antenna with dipoles placed normal to each other as shown in (b). On the bottom: geometry of four antenna configuration: parallel broadside *y*-directed antennas (a), parallel broadside with *x*-directed antennas (b), perpendicular antennas with *y*-directed source and *x*-directed receiver (c) and perpendicular antennas with *x*-directed source and *y*-directed receiver orientation (d).

y-directed receiver orientation (channel 4) [14,18,19] (Fig. 8c). In the present study only the co-polar data with parallel broadside with *y*- and *x*-directed antennas were analyzed.

To obtain an accurate evaluation of the velocity of concrete, a calibration test was performed on a controlled concrete column with a square section of 0.30 m. The column was reinforced with rods spaced about 12 cm apart (Fig. 9). The test was performed in reflection mode, moving the antenna along a profile located at the center of the column. To accurately identify the reflection from the opposite column–air interface, an iron bar, about 0.10 m wide, was positioned on the opposite side of the data acquisition. The position of the reinforced rods and iron bar was clearly detected by the diffraction hyperbola (Fig. 9). The test gave an electromagnetic wave velocity of about 12 cm/ns. A similar velocity was obtained on analyzing the diffraction hyperbola produced by the reinforced rods. This velocity value was used in the migration algorithm, and in the conversion time to space in the data interpretation.

The georadar surveys were carried out on all four sides of the pier in reflection and transillumination modes. The surveys were repeated twice using the same settings before and after the application of the above described mechanical stress.

4.1. Reflection survey

4.1.1. Data acquisition

The reflection survey was carried out on all four sides of the pier, moving the antenna from the bottom to the top of the pier. The use of pad and odometer for data location allowed accurate

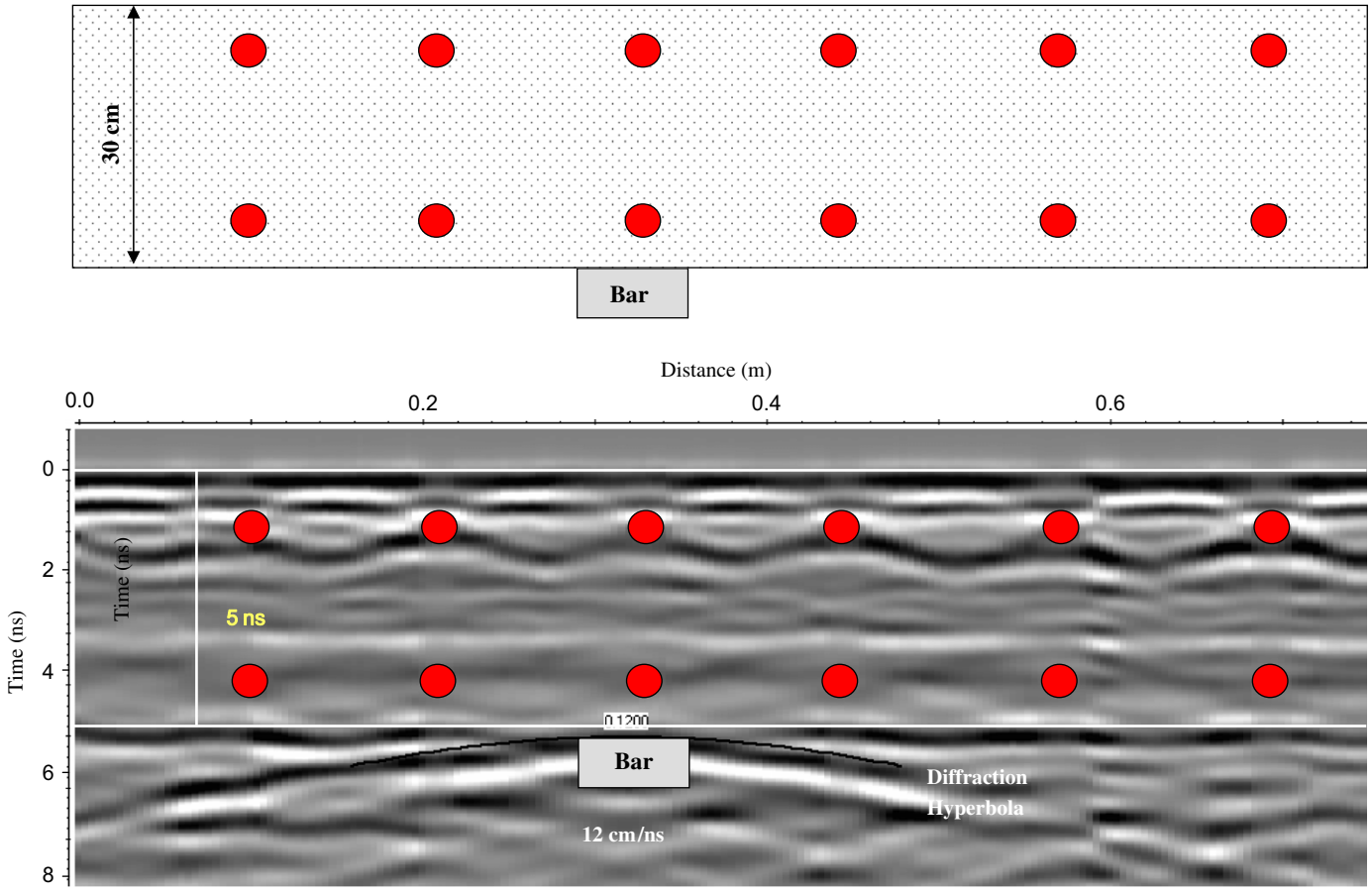

Fig. 9. Top: model of column. Bottom: actual GPR profile from middle of column.

Please cite this article as: Orlando L, et al. Modeling and testing of high frequency GPR data for evaluation of structural deformation. NDT&E Int (2010), doi:10.1016/j.ndteint.2009.11.006

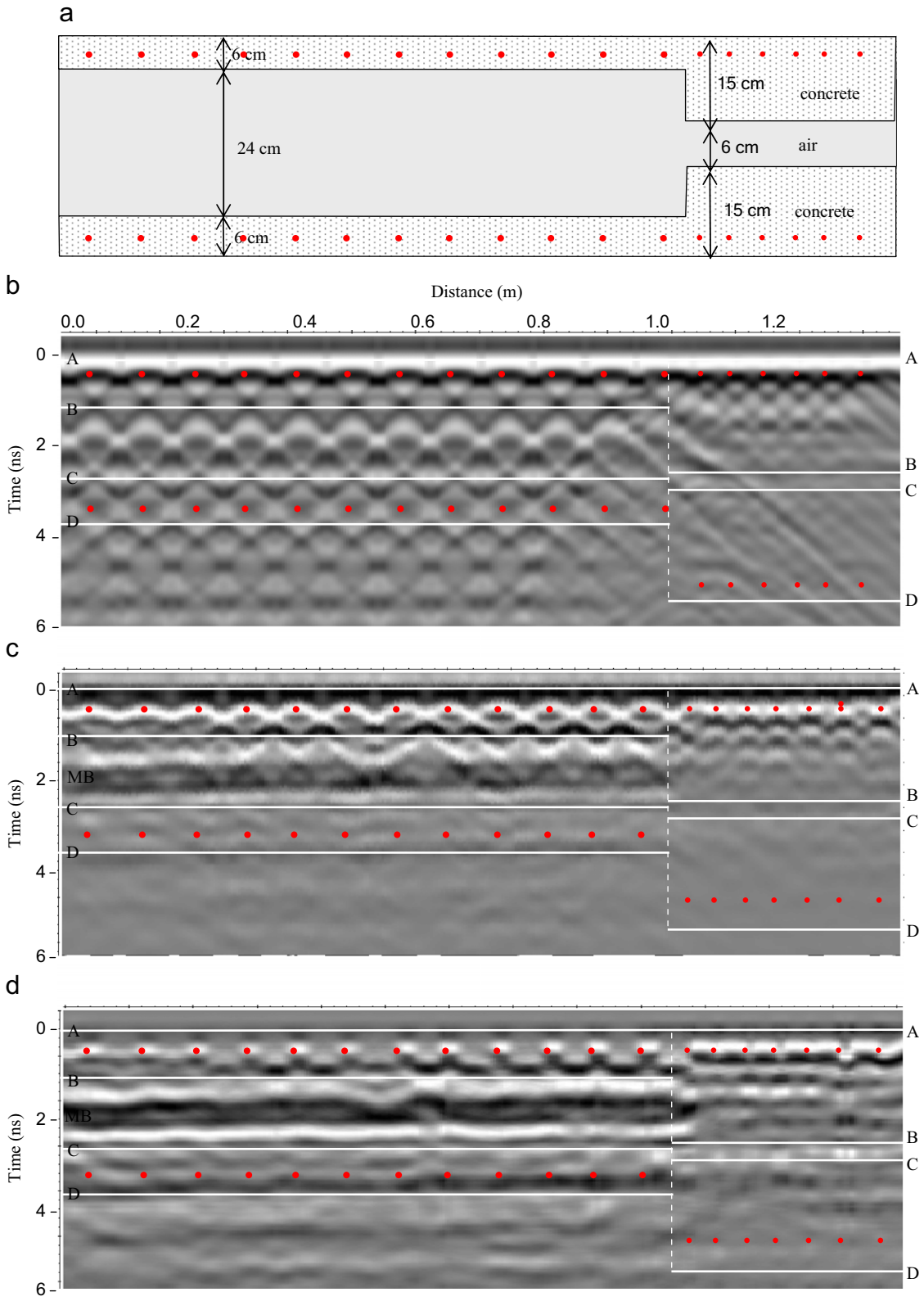

Fig. 10. (a) Pier model with geometry the same as an actual pier. (b) GPR section of model. (c) Actual GPR data acquired at the middle of the pier, using parallel broadside *y*-directed antennas—set to start from the bottom and go to the top during the first survey. (d) Migrated data of (c). The scheme in two travel times of the electric interfaces is shown in white on the GPR profiles. (A and B) Top and bottom of the first concrete layer. (C and D) Top and bottom of the second concrete layer; MB=multiple from (B).

control of the data positions, with a data position error of < 5 mm. On each side of the pier 20 parallel profiles about 1.3 m long and spaced 1.55 cm apart were acquired.

Each profile was acquired with four configuration settings with a trace increment of 0.4 cm, time window of 20 ns and 1024 samples per scan with a sample rate of 0.01953125 ns.

Please cite this article as: Orlando L, et al. Modeling and testing of high frequency GPR data for evaluation of structural deformation. NDT&E Int (2010), doi:10.1016/j.ndteint.2009.11.006

4.1.2. Data processing

The data were processed with the objective of testing the capability of high frequency GPR data to investigate the inner structure of a hollow pier, and to monitor any induced variation in the structural setting of the pier, caused by simulating a seismic event.

The data were processed and analyses were performed on vertical profiles and time slices. Data analysis was performed separately for each survey, and the results were then compared.

The georadar data were processed with a simple sequence: static corrections for the zero time setting, time band-pass filter to remove frequency out of signal band, and migration for the focusing of diffraction energies. Migration was obtained using the Stolt algorithm (1978) with a constant velocity of 12 cm/ns. Gain was applied only for the image editing.

4.1.3. Data analysis

The first interpretation step was to test the capability of the methods to identify the pier's inner features in the georadar image acquired before applying the mechanical strain. Fig. 10c shows the unmigrated profile acquired during the first survey, on the middle part of the pier with a parallel broadside *y*-directed antenna setting. The rods and the inner scheme of the pier transformed into two travel times (dashed lines), are shown on the GPR profiles; the velocity used was 12.24 cm/ns for the concrete and 30 cm/ns for air. The correlation shows that the reflections from the opposite concrete layer have lower reflectivity than the concrete layer near the antenna. In the former the image clearly shows the irregular spacing of the rod position, and the interference of the diffracted energy produced among the rods and air–concrete interfaces. The changes in the inner air space and the iron rod dimensions, which occur 0.96 m from the pier bottom, are clearly detected. The image shows a multiple signal (MB) from interface (B), but only a poor detection of the rods and the concrete layer interface opposite the data acquisition.

On comparing the actual data (Fig. 10c) with the theoretical (Fig. 10b), it can be seen that the signal attenuation in the former is higher than in the theoretical data, and even though the modelling was performed using a Ricker wavelet, with a central frequency equal to the actual data, the actual data have less resolution than the theoretical data.

It is evident from the actual data that data interpretation is a very challenging task because of the complexity of the georadar image. As pointed out in the theoretical data analysis, the main problems of data interpretation lie in the symmetry of the inner geometry, the thin thickness of the layers, the inner hollow filled by air and the proximity of the rods to the antenna. In fact, in the present case the data were acquired in a near-field condition and for geometry very close to the limit of resolution of GPR data frequency.

The rods were focused by the migration algorithm (Fig. 10d), but because of the interference among the rod diffractions themselves, and with the concrete–air interface, several not-actual anomalies are present, and the reflection from interface B appears discontinuous. Thus the image behind the inner air layer appears quite confused, and is not easily interpretable.

In order to carry out the reconstruction of the inner hollow pier we combined the data acquired on all four sides, taking into account only the data related to the pier-half near the antenna position. Fig. 11 shows the section of the middle part obtained combining the profile acquired on side A and the mirror profile acquired on side C.

Fig. 12a shows the inner structure of the pier, and Fig. 12b,c the time slices of pier side C, acquired with parallel and normal broadside *y*-directed antenna respectively. The time slices are from the data acquired before the stress application, and were obtained by stacking the energy of the concrete layer, about 6 cm thick, near the antenna (AB in Fig. 11).

The time slices detect the iron rods extended normal to the profile direction, and their change in dimension at 1 m. The rods extended parallel to the profile direction are not detected by

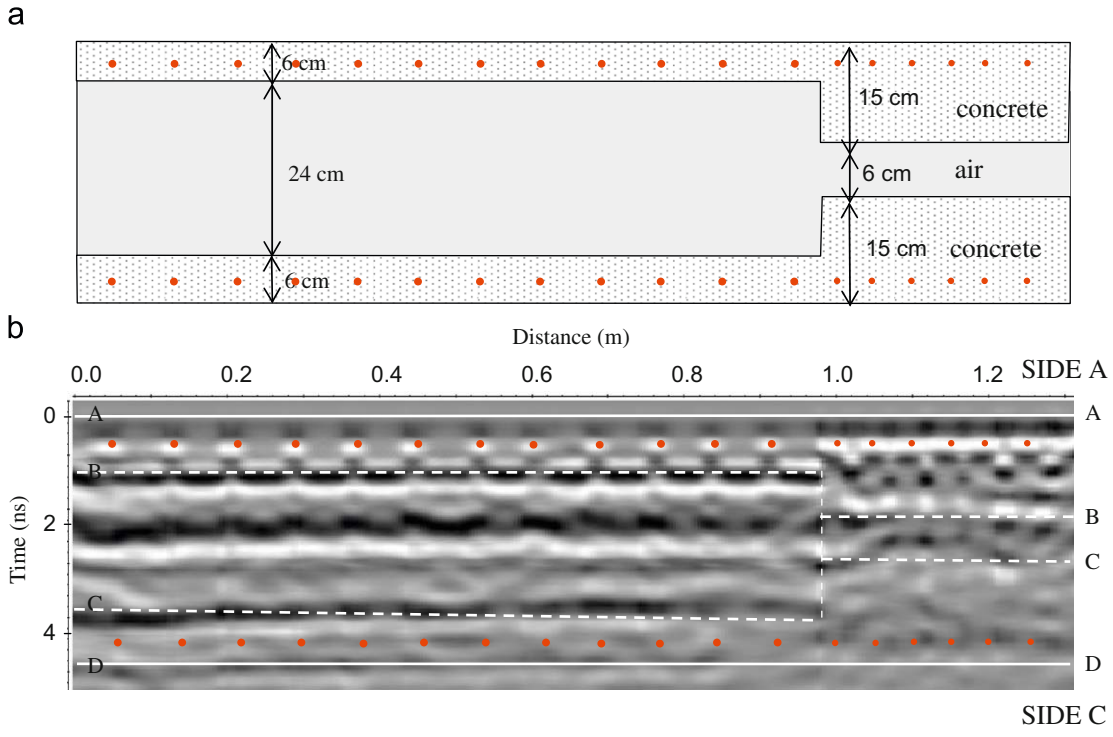

Fig. 11. GPR section from the middle part of pier, obtained combining the profiles acquired on side A and side C, which is the opposite face of (B).

Please cite this article as: Orlando L, et al. Modeling and testing of high frequency GPR data for evaluation of structural deformation. NDT&E Int (2010), doi:10.1016/j.ndteint.2009.11.006

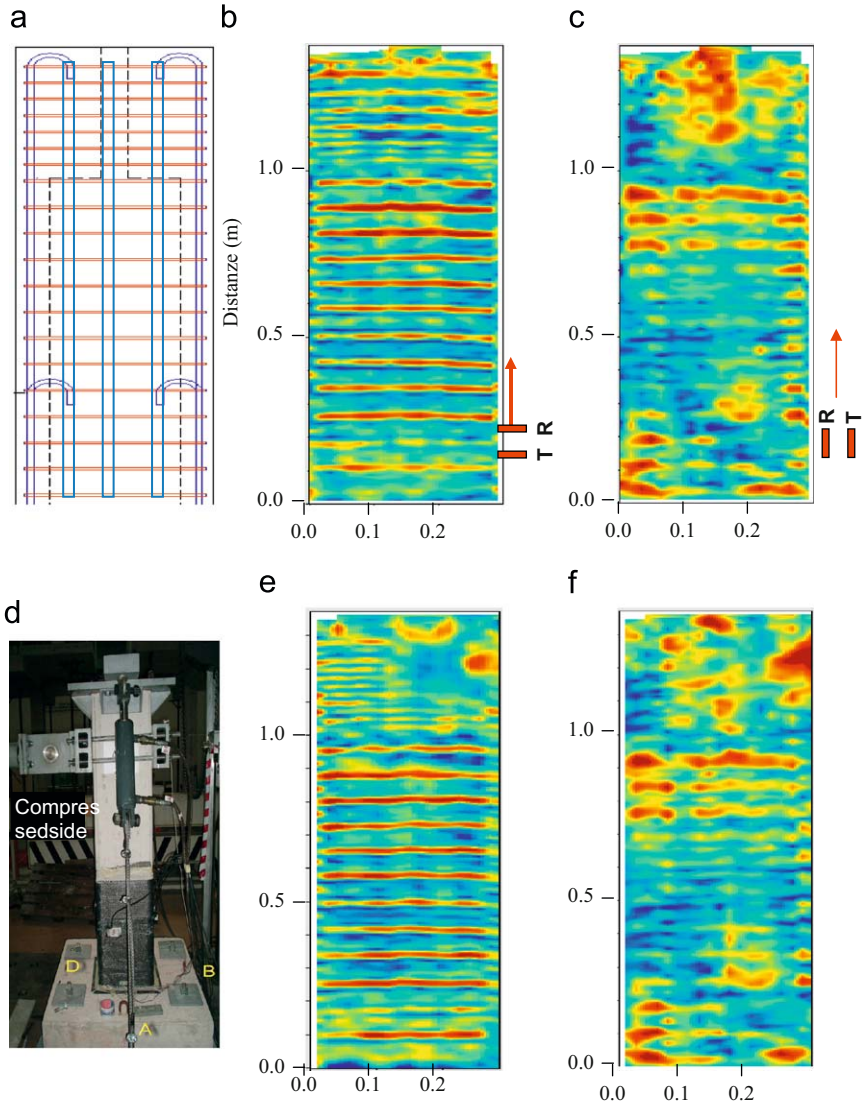

Fig. 12. (a) The inner setting of the pier: blue and red lines depict the rods, the dashed black line the inner limit of the hole. Before the seismic application: time slice of side C of the pier: (b) data acquired with parallel broadside *y*-directed antenna settings. (c) Data acquired with normal broadside *y*-directed antenna settings. (d) The position of the actuator for the strain application. After seismic simulation: time slice of side C of the pier (e) data acquired with parallel broadside *y*-directed antenna settings; (f) data acquired with normal broadside *y*-directed antenna settings. The time slices were obtained by stacking the energy of a 6 cm thick layer. (For interpretation of the references to colour in this figure legend, the reader is referred to the web version of this article.)

either parallel or normal broadside *y*-directed antenna (Fig. 12b, c). These results show that the lack of detection of the parallel rods is not due to the broadside antenna direction but to the lateral sampling, which in this case is 1.55 cm. By combining the time slices of the four sides a 3 D image of the inner hollow pier was obtained. Fig. 13 shows the photograph of pier rods (a), the image combining the GPR profile from the middle part and time slice of data acquired on side B (b) and time slices of sides A and B (c).

4.1.4. Data correlation

The field data (Fig. 14) of the second survey look very similar to those of the first, and are in good agreement with the theoretical data (Fig. 6). However the data acquired after the stress application never show any feature like that produced by the oblique fracture modelled in Fig. 7. Also the qualitative correlation of the corresponding time slices obtained from the two data sets (Fig. 12e, f), acquired before and after the mechanical stress, shows that the mechanical stress does not seem to have induced any qualitatively visible modification of the inner pier structure, except for the reflectivity of the iron rods which is lower in the first survey.

Quantitative modification was observed in the peak frequency (Fig. 4) and e.m. velocity. The peak frequency moved from 1100 to 1200 MHz over time and the velocity increased from 12.2 to 12.5 cm/ns.

The e.m. velocity change between the first and second surveys did not allow any quantitative correlation of the data in the time domain. Moreover we cannot take into account any analysis based on penetration because, for the low conductivity, the concrete layer is a dielectric material with attenuation (α) not depending on frequency:

$$\alpha = \frac{\sigma}{2}\sqrt{\frac{\mu}{\varepsilon}}$$

where σ is the conductivity, μ the permeability and ε the permittivity, and therefore the attenuation is the same for all band frequencies.

Please cite this article as: Orlando L, et al. Modeling and testing of high frequency GPR data for evaluation of structural deformation. NDT&E Int (2010), doi:10.1016/j.ndteint.2009.11.006

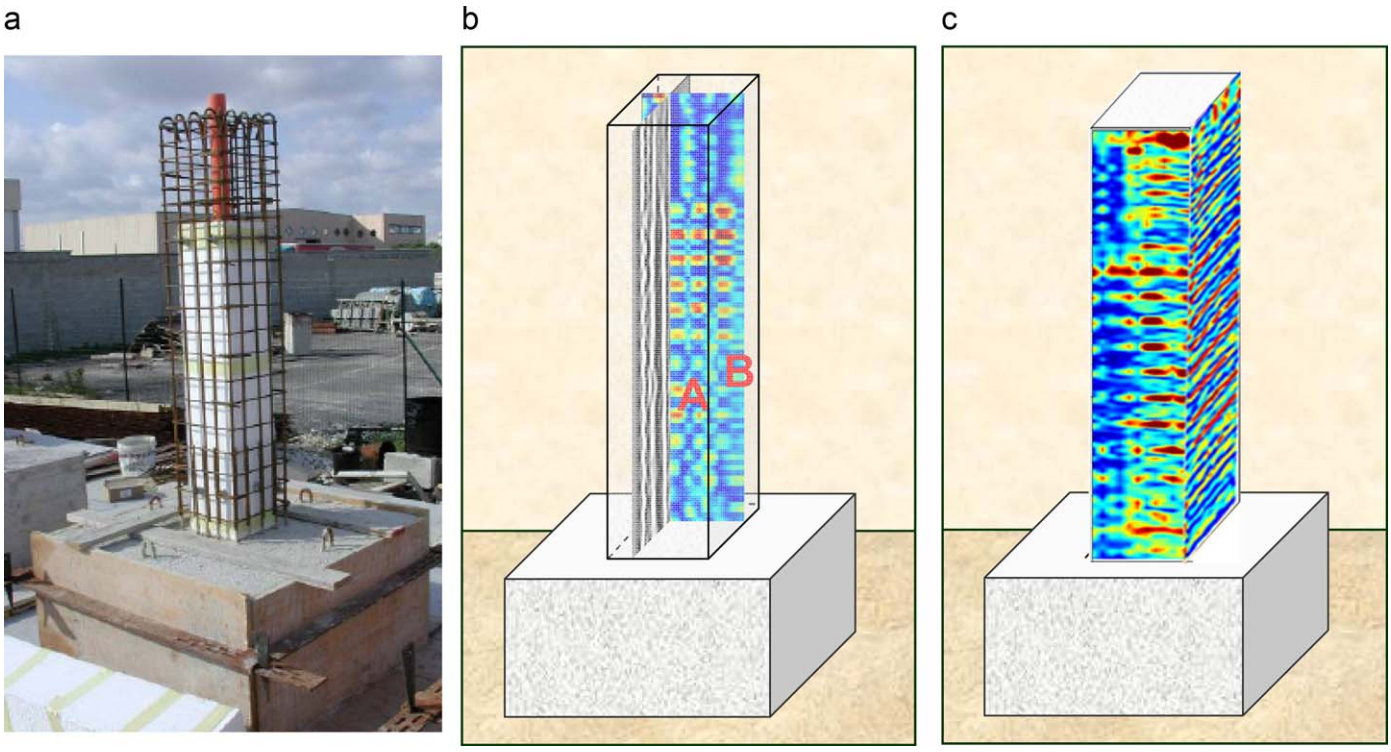

Fig. 13. (a) Structure of iron rods. (b) GPR profile from the middle part, and time slice from the concrete layer near face B. (c) Time slices from faces A and B.

For the evaluation of the micro-cracks we considered that on every interface there will be either diffraction or reflection depending on the ratio of the radius (R) of curvature of the reflecting surface and the wave length (λ) of the signal: cracks $R/\lambda < 1$ produce diffraction and $R/\lambda > 1$ reflection. Therefore, micro-cracks can produce diffraction at high frequency and transmission for low frequency, depending of crack dimensions.

To overcome this problem we considered a frequency attribute that does not depend on wave velocity. This attribute was selected under the hypothesis that if stress induces micro-cracks in the structure, then, depending on the micro-crack dimensions, such cracks could produce signal diffraction of high component signal frequency, which increases high frequency amplitude content. Based on this idea we analyzed the possibility of revealing micro-cracks by frequency analysis.

The spectra were compared using the following normalized relation:

$$\Delta A = \frac{|A_2(f)| - |A_1(f)|}{|A_2(f)|} \quad (1)$$

where ΔA is the normalized amplitude frequency difference of the first and second surveys, $A_1(f)$ the amplitude spectra of the first survey and A_2 of the second. The procedure was (i) stack of 10 traces, (ii) a 1-dimensionl Fourier transform of stacked traces and (iii) calculation of ΔA from (1). The normalized spectra of Fig. 15a,b refer to the reflection data acquired at the center of the pier, gated on a time window of 20 ns. The spectra show an increase in the amplitude of high frequency, 2000–3500 MHz, from the first to the second survey from 0.5 to 1 m window starting from the pier bottom. On referring this result to the pier structure, we found that this zone is located between the end of the carbon fiber and the start of the inner hole reduction (Fig. 15c). This result seems to confirm the effectiveness of carbon fiber for the preservation of a hollow pier from micro-fractures induced by stress.

The higher reflectivity and velocity of the second survey data, with respect to the first, were justified by the increase in air content in the concrete and the modification of the reflection coefficient, probably due to the rods becoming unstuck from the concrete during the applied mechanical stress.

In order to validate this hypothesis it will be necessary to perform more experiments under controlled conditions.

4.2. Transillumination survey

4.2.1. Data acquisition

Transillumination data were collected using two 2 GHz multi-component antennas, one placed on one side of the pier and the other on the opposite side. The first antenna was connected to channel 1 and the second to channel 2. To acquire the data with parallel broadside y-directed configuration, one receiver antenna was rotated 90° with respect to the other. In this way channel 1 acquired the data in the reflection mode and channel 2 in the transillumination mode. The acquisition was performed with one antenna fixed at a point centered on a side of the pier and the other, on the opposite side, was moved so as to acquire data along a profile in continuous mode. Both antennas were positioned at the center of the pier. The mobile antenna was moved from the bottom to the top of pier. This acquisition setting was repeated 12 times for each side, the offset of the fixed antenna was 0.10 m. In this way 12 profiles for each side of the pier were acquired. The data acquisition parameters were a trace increment of 0.4 cm, time window of 20 ns and 1024 samples per scan.

4.2.2. Data processing

The transillumination data were processed with zero time setting, gain and filter. Fig. 16 shows, at the top, an example of the data of the first survey, and the corresponding example of the second, with the transmitter on the C side and receiver on the A

Please cite this article as: Orlando L, et al. Modeling and testing of high frequency GPR data for evaluation of structural deformation. NDT&E Int (2010), doi:10.1016/j.ndteint.2009.11.006

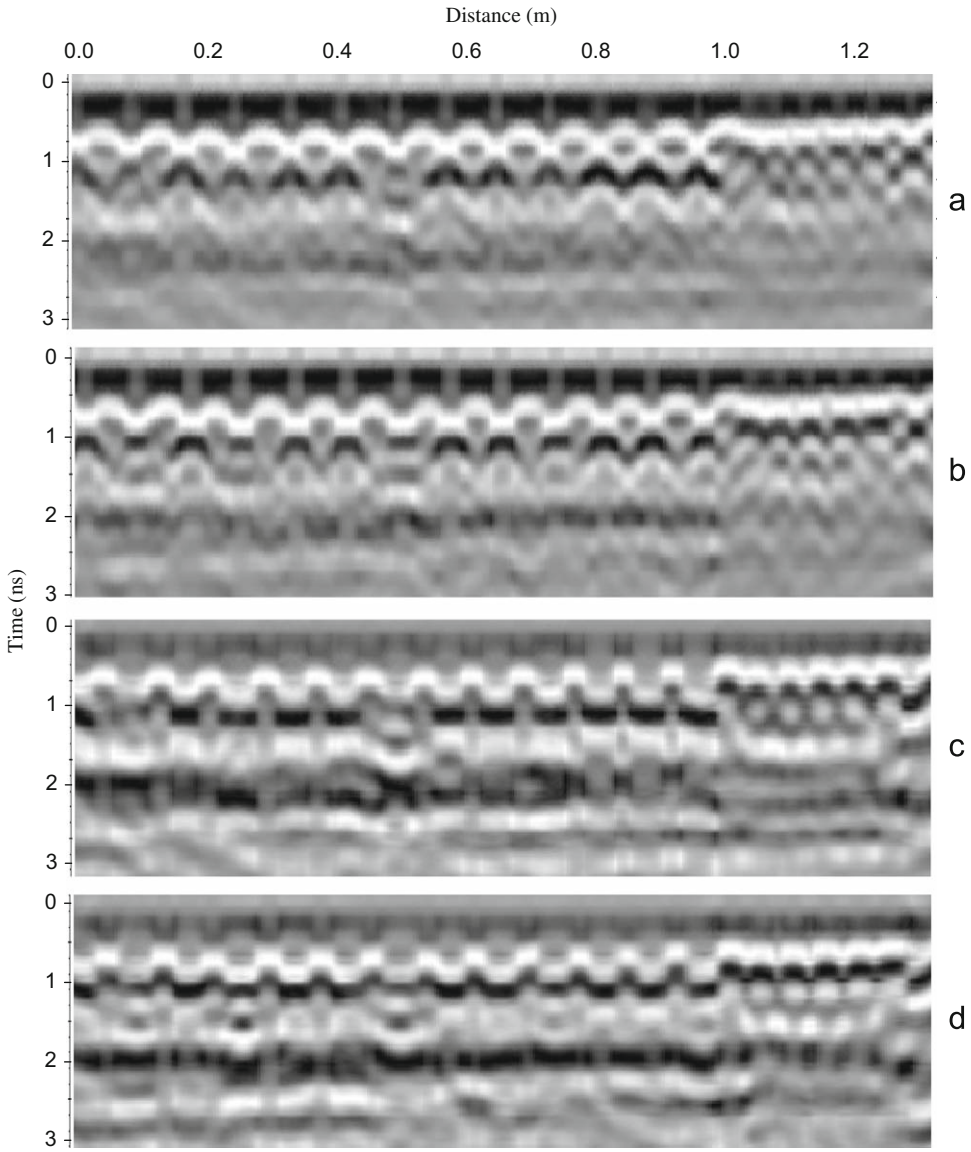

Fig. 14. Unmigrated profiles acquired before (a) and after (b) the seismic stress application. Migrated profiles acquired before (c) and after (d) seismic stress. The data are referred to parallel broadside *y*-directed antenna settings.

side, at the bottom. The high frequency undulation of the first arrivals is due to the rods, while the bad quality data occurring at 1.1 m from the bottom is located in correspondence with the reduced inner air inter-space. The first arrivals show a change in wave shape and an increase in signal amplitude from the first survey to the second. This was probably due mostly to the micro-cracks induced by the mechanical stress, and not by any variation in environmental conditions (humidity, temperature, coupling of antenna, etc.), the pier being located inside the laboratory and the measurements performed in the same season. For each transmitter position we performed and compared the values of the first break of the first and second surveys. The picking was done automatically by correlating the maximum energies. In most cases the travel times of the second survey were shorter than the first one, and the variation is higher in the data acquired on sides B and D (Fig. 17), probably depending on the strain direction as shown by the photograph in the middle of Fig. 17. The time variation over time was justified by the increase in the air content within the concrete, due to the loosening and separation of the iron rods from the concrete, induced by stress in the second survey. These results are in good agreement with those from the GPR reflection data.

Because of the complexity of the pier geometry, and the small dimensions of the concrete, we are of the opinion that the error in the first break picking and the high variation in time between concrete and rods preclude the use of the data for tomographic inversion, which is able to highlight microvariations induced by seismic stress.

5. Conclusions

This study addressed the problem of verifying the capability of a high frequency GPR method for the detection and monitoring of deformation induced by strain on a hollow pier of the type normally used for viaducts and bridges in Europe. The results were validated by tests carried out on a purposely built hollow pier, scale 1:5, constructed in our laboratory.

GPR data, acquired before and after the application of controlled strain, show that 2 GHz GPR data are a useful tool for

Please cite this article as: Orlando L, et al. Modeling and testing of high frequency GPR data for evaluation of structural deformation. NDT&E Int (2010), doi:10.1016/j.ndteint.2009.11.006

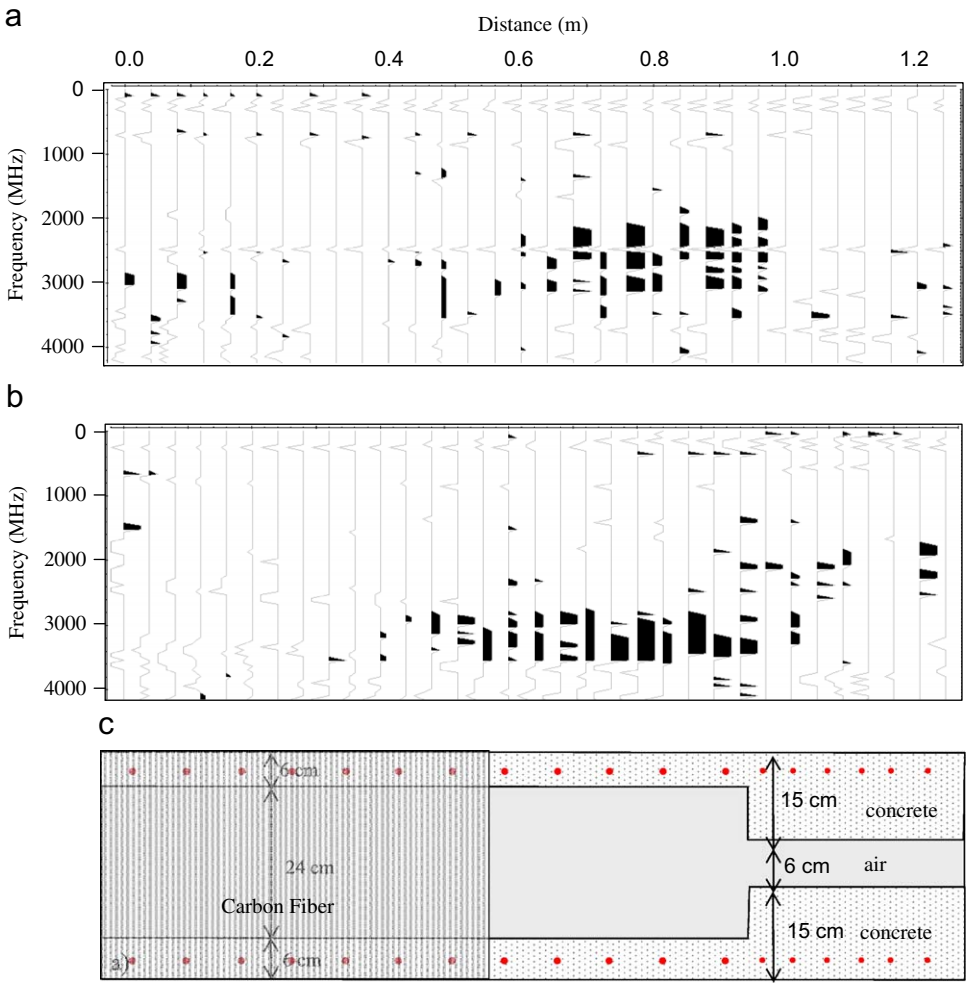

Fig. 15. Normalized spectra obtained using relation 1 on 10 stack traces of two profiles (a, b) acquired at the middle of the pier, with parallel broadside *y*-directed antenna settings. (c) Scheme of hollow pier with location of optic fiber.

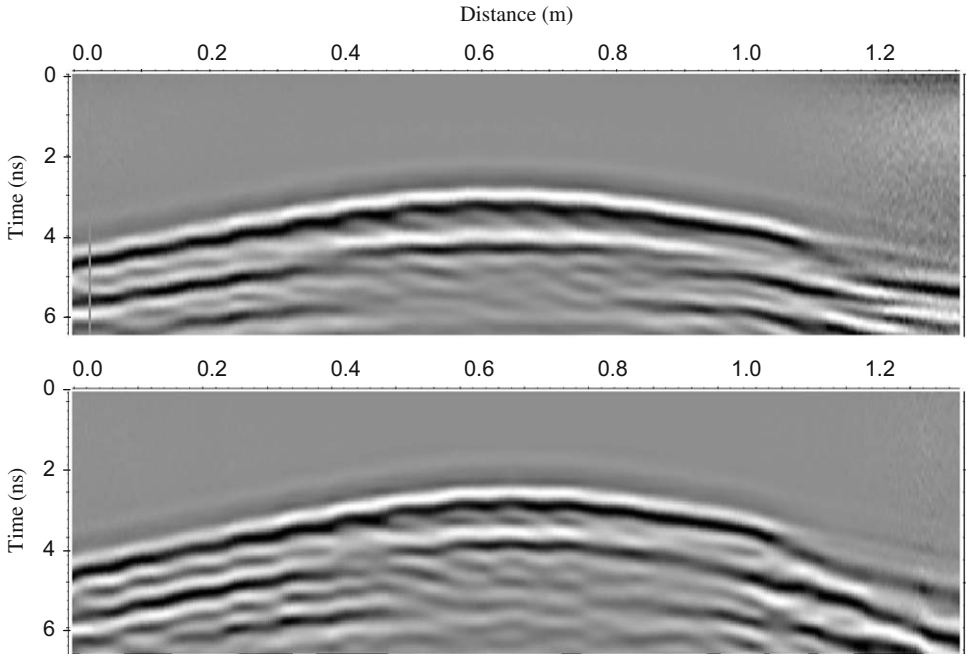

Fig. 16. Top—transillumination data acquired during the first survey. Bottom—data of the second survey.

Please cite this article as: Orlando L, et al. Modeling and testing of high frequency GPR data for evaluation of structural deformation. NDT&E Int (2010), doi:10.1016/j.ndteint.2009.11.006

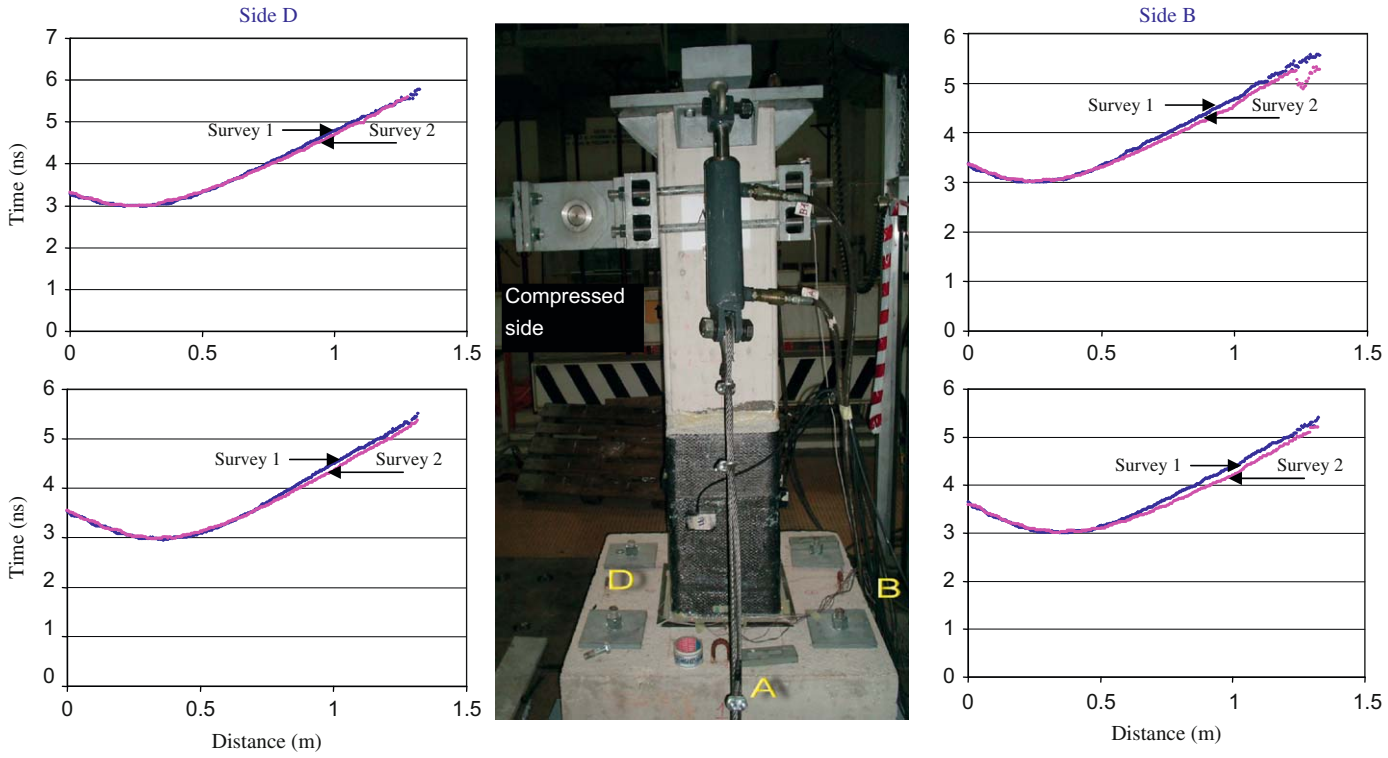

Fig. 17. First break picking of two transillumination data, located with the fixed antenna in two different positions and referred to the first and second surveys, acquired on side D (left) and side B (right). In the middle, the photograph of the stress simulation.

reconstructing the inner structures of a hollow pier, even though the dimensions of the concrete layer were at the limit of antenna frequency resolution and the data fall, for the most part, in a near-field zone.

The study has shown that the theoretical model is a very important tool for the correct interpretation of such complex structures, which, because of interference of diffraction among the rods themselves, and with concrete–air interfaces, several not-actual anomalies are present in the GPR image. The migration code applied to the data did not improve the image quality very much. Moreover the presence of an inner hole does not allow the investigation of the pier as a whole. Thus, for a complete reconstruction of the inner pier setting, it is necessary to combine data acquired on all four sides of the pier, using them together for an interpretation on vertical profiles and time slices.

A simple qualitative correlation of the profiles and time slices acquired before and after the application of stress did not reveal any significant variation of the inner pier setting, but it did reveal a variation in velocity and reflection amplitude, both of which were higher in the second survey. The transillumination data analysis confirms these results, giving an increase in velocity and reflectivity of the second survey with respect to the first.

The velocity and amplitude variations were most likely justified as due to the loosening of the rods within the concrete, as there were no variations in environmental conditions (humidity, temperature, coupling of antenna, etc.) over time.

Velocity variation occurred after the first survey did not allow a quantitative evaluation of the deformation induced by stress in the time domain, but we have been able to show that the frequency amplitude attribute, not depending on time, is a useful tool for this purpose. In fact, the analysis of the normalized difference of the frequency spectra of the first and second surveys highlights that, in the unprotected pier zone, traces acquired by optic fiber during the strain are characterized by high frequency content. The increase in the high frequency amplitude was justified by an increase in scattered high frequency. We feel that the justification of these results lies in the loosening of the rods from the concrete and the presence of micro-cracks induced by strain, both of which can produce diffraction of high frequency components. This result seems to confirm the effectiveness of carbon fiber for the preservation of a hollow pier from micro-cracks induced by stress.

Acknowledgments

I wish to thank Engineer Gerardo De Cano for permitting the georadar survey, and Francesco Pugliese and Francesco Di Biagio for helping with the data acquisition.

References

[1] Binda L, Saisi A, Tiraboschi C, Valle S, Colla C, Forde M. Application of sonic and radar tests on the piers and walls of the Cathedral of Noto. Construction and Building Materials 2003;17(8):613–27.
[2] Hugenschmidt J. Concrete bridge inspection with a mobile GPR system. Construction and Building Materials 2002;16(3):147–54.
[3] Cardarelli E, de Nardis R. Seismic refraction, isotropic anisotropic seismic tomography on an amcient monument (Antonino and Faustino temple AD 141). Geophysical Prospecting 2001;49:228–40.
[4] Cardarelli E, Marrone C, Orlando L. Evaluation of tunnel stability using integrated geophysical methods. Journal of Applied Geophysics 2003;52(2–3):93–102.
[5] Pérez-Gracia V, García F, Pujades LG, Drigo RG, Di Capua D. GPR survey to study the restoration of a Roman monument. Journal of Cultural Heritage 2008;9(1):89–96.
[6] Pérez-Gracia V, García García F, Rodriguez Abad I. GPR evaluation of the damage found in the reinforced concrete base of a block of flats: a case study. NDT & E International 2008;41(5):341–53.
[7] Pérez-Gracia V, Caselles O, Clapés J, Osorio R, Canas JA, Pujades LG. Radar exploration applied to historical buildings: a case study of the Marques de Lió Palace, in Barcelona (Spain). Engineering Failure Analysis 2009;16(4):1039–50.
[8] Binda L, Saisi A, Tiraboschi C. Application of sonic tests to the diagnosis of damaged and repaired structures. NDT & E International 2001;34(2):123–38.

Please cite this article as: Orlando L, et al. Modeling and testing of high frequency GPR data for evaluation of structural deformation. NDT&E Int (2010), doi:10.1016/j.ndteint.2009.11.006

[9] Trela Ch Wöstmann J, Kruschwitz S. Contribution of radar measurements to the inspection and condition assessment of railway bridges—case study at a historic masonry arch bridge in Oleśnica/Poland. In: De Wilde WP, editor. High performance structures and materials IV. Vrije Universiteit Brussels, Belgium, CA, Brebbia, Wessex Institute of Technology, UK; 2008.
[10] Masini N, Nuzzo L, Rizzo E. GPR investigations for the study and the restoration of the rose window of Troia Cathedral (southern Italy). Near Surface Geophysics 2007;5(5):287–300.
[11] Hugenschmidt J, Mastrangelo R. GPR inspection of concrete bridges. Cement and Concrete Composites 2006;28(4):384–92.
[12] Liu Dun-wen, Deng Yu, Yung Fei, Xu Guo-yuan. Non destructive testing for crack of tunnel lining using GPR. Journal of Central South University of Technology 2005;12:120–4.
[13] Porsani JL, Sauck WA, Júnior AOS. GPR for mapping fractures and as a guide for the extraction of ornamental granite from a quarry: a case study from southern Brazil. Journal of Applied Geophysics 2006;58(3):177–87.
[14] Orlando L. Using GPR to monitor cracks in a historical building. In: Proceeding of the 2007 4th international workshop on advanced ground penetrating radar, June '07 Naples, Italy, 2007. p. 45–7.
[16] Giannopoulos, A. GprMax2D V 1.5, 2003 (Electromagnetic simulator for ground probing radar, the software is available at 〈www.gprmax.org〉).
[15] Orlando L, Slob E. Using multicomponent GPR to monitor cracks in a historical building. Journal of Applied Geophysics 2009;67:327–34.
[17] Stolt RH. Migration by Fourier transform. Geophysics 1978;43:23–48.
[18] van der Kruk J, Wapenaar CPA, Fokkema JT, van den Berg PM. Improved three-dimensional image reconstruction technique for multi-component ground penetrating radar data. Subsurface Sensing Technologies & Applications 2003;4:61–99.
[19] van der Kruk J, Wapenaar CPA, Fokkema JT, van den Berg PM. Three-dimensional imaging of multicomponent ground-penetrating radar data. Geophysics 2003;68(4):1241–54.

Please cite this article as: Orlando L, et al. Modeling and testing of high frequency GPR data for evaluation of structural deformation. NDT&E Int (2010), doi:10.1016/j.ndteint.2009.11.006